

# Full-Hexacyanometallate Aqueous Redox Flow Batteries Exceeding 1.5 V in an Aqueous Solution

Ji-Eun Jang, Ryeong-ah Kim, S. Jayasubramaniyan, Chanhee Lee, Jieun Choi, Youngdae Lee, Sujin Kang, Jaechan Ryu, Seok Woo Lee, Jaephil Cho, Dong Woog Lee, Hyun-Kon Song, Wonyoung Choe, Dong-Hwa Seo,\* and Hyun-Wook Lee\*

Aqueous redox flow batteries (RFBs) have attracted significant attention as energy storage systems by virtue of their inexpensive nature and long-lasting features. Although all-vanadium RFBs exhibit long lifetimes, the cost of vanadium resources fluctuates considerably, and is generally expensive. Iron–chromium RFBs take advantage of utilizing a low-cost and large abundance of iron and chromite ore; however, the redox chemistry of Cr<sup>II/III</sup> generally involves strong Jahn–Teller effects. Herein, this work introduces a new Cr-based negolyte coordinated with strong-field ligands capable of mitigating strong Jahn–Teller effects, thereby facilitating low redox potential, high stability, and rapid kinetics. The balanced full-cell configuration features a stable lifetime of 500 cycles with energy density of 14 Wh L<sup>-1</sup>. With an excessive posolyte, the full-cell can attain a high energy density of 38.6 Wh L<sup>-1</sup> as a single electron redox process. Consequently, the proposed system opens new avenues for the development of high-performance RFBs.

additionally, they have low maintenance and cost.<sup>[1,2]</sup> However, the current lithium-ion battery (LIB) technology might not be chosen as an ideal candidate to replace active materials in the positive and negative electrodes in grid energy storage because faded LIBs result from the degradation of active materials (cathode and anode) or the dried electrolyte. When contemplating long-term operations or replacing a defective component, LIB maintenance entails rather significant expenses and complex procedures. In this regard, aqueous redox flow batteries (RFBs) have been widely employed as an alternative for economical ESSs.<sup>[3–5]</sup> One noticeable advantage of aqueous systems is their very high dielectric constant, allowing soluble redox couples to dissolve with

## 1. Introduction

Sustainable energy storage systems (ESSs) have received a great deal of attention to satisfy emerging demands at grid-scale without compensation for large-scale and long-time operation;

large quantities in an aqueous solution with dissociation.<sup>[6]</sup> The high solubility also benefits to increase the available energy densities and the output current would be controlled by the size of the electrode stacks in RFBs.<sup>[7]</sup> Of course, aqueous systems are advantageous in many aspects of: they are inexpensive, environmentally benign, and highly soluble rather than the use of organic liquid-based RFBs.<sup>[8,9]</sup> As shown in **Figure 1a** replacing or rebalancing negolytes and posolytes can be readily altered while maintaining infra-tank and pump systems; such properties are well-suited for stationary energy storage. All-vanadium RFBs have been widely studied since the same elements are employed in both the negolyte (V<sup>II/III</sup>) and posolyte (V<sup>IV/V</sup>) and since such systems feature long calendar and cycle lives with more than 200 000 cycles.<sup>[10–12]</sup> Nevertheless, the price of vanadium source, V<sub>2</sub>O<sub>5</sub>, has been highly fluctuated up to 28.8 USD lb<sup>-1</sup> at the end of 2018, resulting in high costs and performance as 1000 USD kWh<sup>-1</sup> approximately.<sup>[13]</sup>

J.-E. Jang, R.-ah Kim, S. Jayasubramaniyan, C. Lee, J. Choi, Y. Lee, S. Kang, J. Ryu, J. Cho, D. W. Lee, H.-K. Song, D.-H. Seo, H.-W. Lee  
School of Energy and Chemical Engineering  
Ulsan National Institute of Science and Technology (UNIST)  
Ulsan 44919, Republic of Korea  
E-mail: dseo@unist.ac.kr; hyunwooklee@unist.ac.kr

S. W. Lee  
School of Electrical and Electronic Engineering  
Nanyang Technological University  
Singapore 639798, Singapore

W. Choe  
Department of Chemistry  
UNIST  
Ulsan 44919, Republic of Korea

The ORCID identification number(s) for the author(s) of this article can be found under <https://doi.org/10.1002/aenm.202300707>

© 2023 The Authors. Advanced Energy Materials published by Wiley-VCH GmbH. This is an open access article under the terms of the Creative Commons Attribution-NonCommercial License, which permits use, distribution and reproduction in any medium, provided the original work is properly cited and is not used for commercial purposes.

The concept of iron-chromium RFBs using ferrous/ferric (Fe<sup>II/III</sup>) and chromous/chromic (Cr<sup>II/III</sup>) ions is the first chemistry taking advantage of low cost and widely abundant iron and chromite ore.<sup>[2,14]</sup> These Fe<sup>II/III</sup> redox couples are expected to be more stable as a posolyte with a combination of cyanide ligands that have extensively used to a posolyte material in RFB reference.<sup>[15–20]</sup> However, the redox chemistry of Cr<sup>II/III</sup> in chromium-based negolytes generally involves strong Jahn–Teller effects due to the unequal occupation of electrons in e<sub>g</sub> orbitals

DOI: 10.1002/aenm.202300707

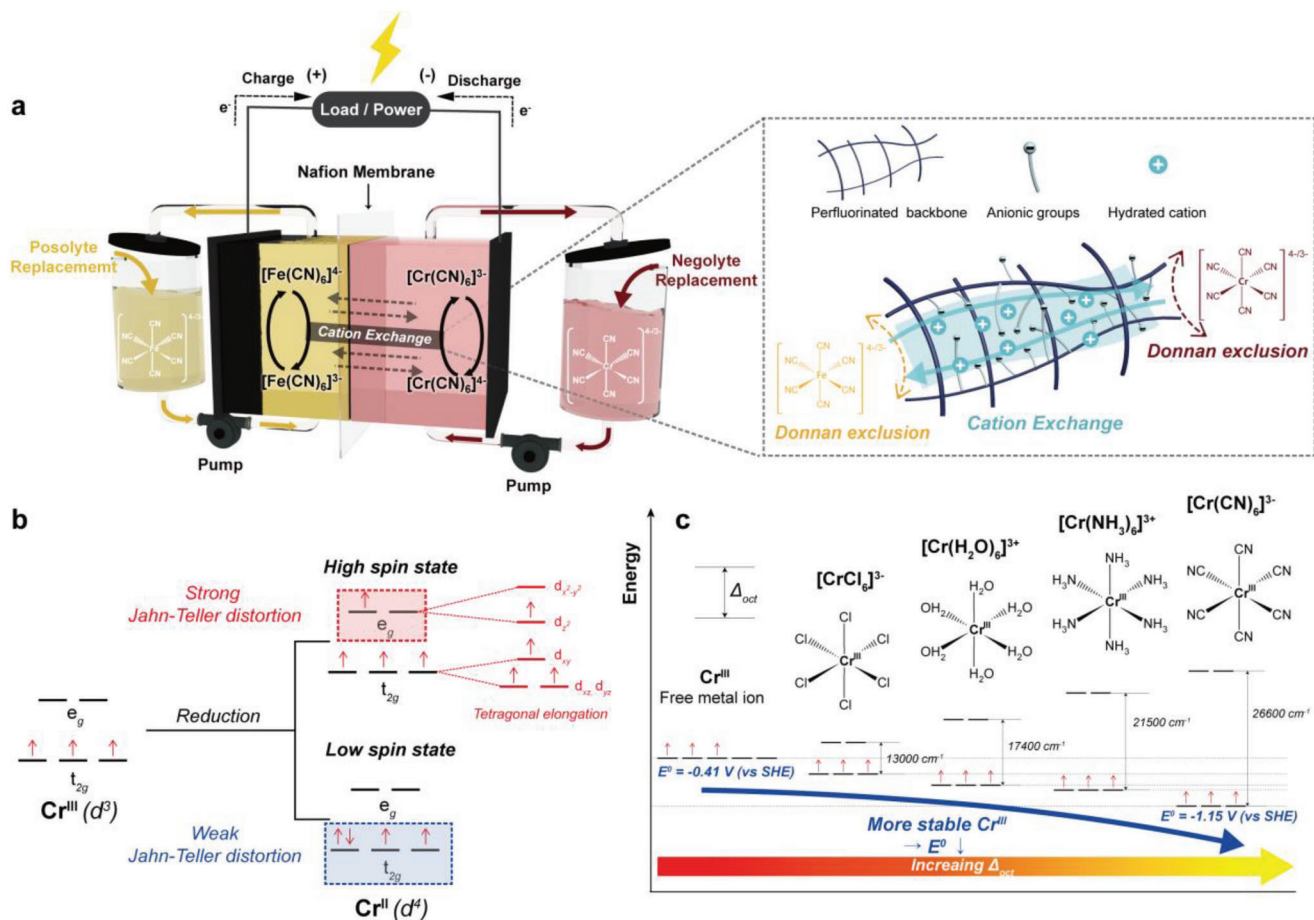


**Figure 1.** Cell configuration and  $d$ -orbital splitting for different chromium octahedral complexes. a) Cell schematic of the negolyte of  $[\text{Cr}(\text{CN})_6]^{4-/3-}$  paired with the posolyte of  $[\text{Fe}(\text{CN})_6]^{4-/3-}$ . The negolyte (red) and posolyte (yellow) are circulated through the pump. The active electrolytes can be replaced or rebalanced when the system is degraded. The arrows in the middle of the diagram indicate cation migration across the Nafion membrane. Mobile cations of sodium are readily transported through the membrane. On the other hand, hexacyanometallate anions of  $[\text{Cr}(\text{CN})_6]^{4-/3-}$  and  $[\text{Fe}(\text{CN})_6]^{4-/3-}$  are excluded by Donnan exclusion effects. b) Jahn–Teller effects of  $\text{Cr}^{\text{II}} (d^4)$  octahedral complex. c)  $d$ -orbital splittings and the reduction potentials of chromium-based octahedral complexes.

of high-spin  $\text{Cr}^{\text{II}} (d^4)$  as shown in Figure 1b. This can lead to simultaneous splitting of the electronic states and a symmetry-lowering distortion. This phenomenon limits the electrochemical reactions as a low current density and energy efficiency, resulting in the sluggish kinetics of the  $\text{Cr}^{\text{II/III}}$  redox couple ( $k_0 < 10^{-6}$ )<sup>[18,21,22]</sup> and low Coulombic efficiency, which is corroborated by a severe hydrogen evolution reaction (HER) arising from the low reduction potential ( $-0.41$  V versus SHE) under acidic conditions.<sup>[23]</sup> Interestingly, the  $d^4$  electron configuration of  $\text{Cr}^{\text{II}}$  can alter its spin states from high-spin to low-spin depending on the increase of the energy gap ( $\Delta_0$ ) between  $e_g$  and  $t_{2g}$  orbitals. Coordination compounds composed of a metal ion and ligands offer the benefit of  $\pi$  interactions, which facilitate dramatic effects on the triply degenerate  $t_{2g}$  orbitals.<sup>[24]</sup> Ligands such as carbonyls (CO) and cyanides ( $\text{CN}^-$ ) are  $\pi$  acceptors with empty orbitals that can interact with metal  $d$  orbitals in a  $\pi$  fashion, leading to the stabilization of  $t_{2g}$  orbitals. It has been suggested that the significant electronic stabilization is beneficial to stable  $\text{Cr}^{\text{II/III}}$  redox reactions enabled by the low-spin configuration of  $\text{Cr}^{\text{II}}$ . As shown in Figure 1c, the energy split between  $e_g$  and  $t_{2g}$

orbitals can increase from the free metal ion state to coordination with a strong-field ligand, playing a crucial role in shifting a redox potential more negative figures according to spectrochemical series.<sup>[25]</sup> In particular, when  $\text{Cr}^{\text{III}}$  changes its oxidation state to  $\text{Cr}^{\text{II}}$  at a high-spin state, electrons are transferred into the  $e_g$  orbitals, whereas electron transfer can occur into  $t_{2g}$  orbitals in the coordination complex covalent with strong-field ligands, manipulating the redox potential of  $\text{Cr}^{\text{II/III}}$  via the use of suitable ligands and simultaneously mitigating strong Jahn–Teller effects.

Although various studies have provided some negolytes in a chromium-based system, there is a need for negolytes containing low-redox-potential with fast kinetics and stable cyclability.<sup>[17,18,26–30]</sup> Bae et al. showed that chromium-ethylenediaminetetraacetic acid (Cr-EDTA) can exhibit a low reduction potential ( $-0.99$  V versus SHE) with reversible cathodic and anodic processes. However, the designed battery has shown slow kinetics operated at very low current density of  $2.5$  mA  $\text{cm}^{-2}$ , and a very low energy efficiency of less than 7% due to the large overpotential of chromium-based redox couples.<sup>[26,27]</sup> Slow kinetics inhibit the power density of batteries and occur

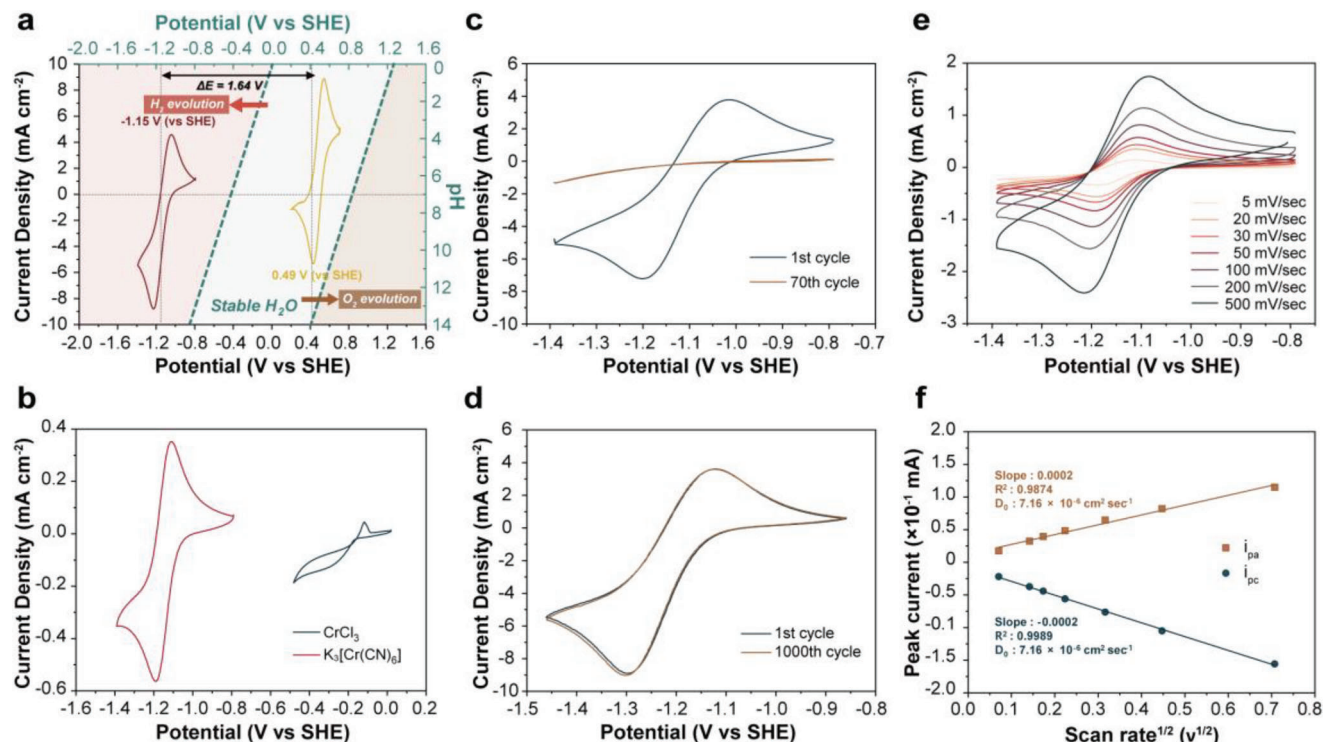


**Figure 2.** Electrochemical characterization of  $K_3[Cr(CN)_6]$ . a) CV of  $[Cr(CN)_6]^{4-/3-}$  redox species (brown) and the counterpart of  $[Fe(CN)_6]^{4-/3-}$  (yellow) at a scan rate of  $20\text{ mV s}^{-1}$  on a glassy carbon electrode. The blue dashed lines denote the thermodynamic reduction potentials of the HER and OER, which depend on pH. b) CV of  $5 \times 10^{-3}\text{ M}$   $[Cr(CN)_6]^{4-/3-}$  redox species (red) and the redox behavior of  $CrCl_3$  coordinated with weak-field ligands of chlorine (black) at a scan rate of  $20\text{ mV s}^{-1}$ . c,d) Stability test of  $0.1\text{ M}$   $K_3[Cr(CN)_6]$  with the different supporting electrolytes of  $1\text{ M}$  NaCl (c) or  $1\text{ M}$  NaCN (d) at  $20\text{ mV s}^{-1}$ . e) CV curves of  $5 \times 10^{-3}\text{ M}$   $[Cr(CN)_6]^{4-/3-}$  redox species at different scan rates from 5 to  $500\text{ mV s}^{-1}$ . f) Relationship between peak currents and corresponding scan rates of  $K_3[Cr(CN)_6]$ .

in the comparable reaction of hydrogen evolution, although chromium complexes have merits of low redox potential, allowing for an overall high voltage. Marshak et al. introduced 1,3-propylenediaminetetraacetic acid chelated chromium (Cr-PDTA) as a negolyte material using a strategy of chelating ligands. The full-cell couple with the posolyte,  $[Fe(CN)_6]^{4-/3-}$  showed a high discharging potential of approximately 1.5 V and an improved energy efficiency of 78.1% during cycling at  $\pm 100\text{ mA cm}^{-2}$ , which provides the best performance among the new chromium-based RFBs. However, such cycle life of 70 still needs to be ameliorated. Chen et al. found various chromium complexes for Cr-based RFBs, such as Cr-bipyridine ( $[Cr(bipy)_2(H_2O)_2]^{3+}$ ), Cr-dipicolinic acid ( $[Cr(DPA)_2]^-$ ), Cr-iminodiacetate ( $[Cr(IDA)_2]^-$ ), and chromium 3-((2,6-bis(ethoxycarbonyl)pyridin-4-yl)oxy)-*N,N,N*-trimethylpropan-1-aminium bromide ( $[Cr(f-DPA)_2]^+$ ).<sup>[18]</sup> This work assessed that the charge transfer kinetics, stability, and solubility of a complex would be corroborated by the suitable molecular design. Goeltz et al. reported a hexacyanochromate redox reaction based on a single cyclic voltammogram (CV) of  $[Cr(CN)_6]^{4-/3-}$ .<sup>[31]</sup> In general, the Cr(II) complex is less stable than Cr(III) complex due to weaker bond strength between Cr(II) and ligands because the formation constant of Cr(II) cyanide is smaller than that of the Cr(III) cyanide complex. Consequently, it is crucial to suppress the undesirable decomposition of the Cr(II) complex during electrochemical cycling of RFBs. Therefore, the better designs of material chemistry are indubitably required in

order to resolve the performance issues associated with the aforementioned systems.

In this work, we introduce a new Fe-Cr RFB system coordinated by strong-field cyanide ligands to mitigate strong Jahn–Teller effects for high-energy and stable performances. Chromium complexes coordinated with strong-field cyanides can allow low redox potentials compared to complexes coordinated with weak-field ligands due to the electron transfer to  $t_{2g}$  orbitals rather than  $e_g$  orbitals. Since this system is introduced for the first time, we have carefully evaluated diverse assessment methods for the unique features with low redox potential, high stability, and fast kinetics below the potential of HER as shown in Figure 2a. A thermodynamic analysis of the redox reaction energetics using density functional theory (DFT) calculations suggests that the  $[Cr(CN)_6]^{4-}$  complex is preferentially associated with low-spin states relative to complexes coordinated with weak-field ligands, facilitating a stable and fast redox reaction. In order to enable further development of redox flow system, we matched the negolyte with a  $K_3[Fe(CN)_6]$  posolyte as a full cell and performed various investigations to confirm the proper redox at different state of charges (SOCs). Benefiting from the aforementioned uniqueness, this hexacyanometalate-based RFB is capable of reversible redox reactions with relatively high potential as an aqueous system taking advantage of the low potential of  $[Cr(CN)_6]^{4-/3-}$  and improved cycling performance at high current densities. Furthermore, we expand on the considerable degradation mechanisms

that play a crucial role in governing the kinetics and stability of the reaction and provide important insights into the design of a stable RFB.

## 2. Results

### 2.1. Electrochemical Properties of Hexacyanochromate with Respect to Low Redox Potential, High Stability, and Fast Kinetics

Facile synthetic  $K_3[Cr(CN)_6]$  was employed as a source of  $[Cr(CN)_6]^{4-/3-}$  in our experiment; this enabled us to take advantage of the low chemical cost of chromium(III) acetate, which is beneficial compared to the onerous price of commercially available  $K_3[Cr(CN)_6]$  (Sigma–Aldrich, 99.99%). X-ray diffraction (XRD) profiles in Figure S1 (Supporting Information) reveal that as-synthesized  $K_3[Cr(CN)_6]$  corresponds to the XRD patterns of both commercialized  $K_3[Cr(CN)_6]$  and PDF 00-027-1350. CVs in Figure 2a,b show reversible redox reactions of  $[Cr(CN)_6]^{4-/3-}$  anions, which possess the reduction and oxidation peaks at  $-1.19$  and  $-1.11$  V versus SHE, respectively. Whereas CV of  $Cr^{II/III}$  in  $CrCl_3$  redox reaction denotes serious irreversibility with a considerably small oxidation peak near  $-0.11$  V and a negligible reduction peak, even at the same scan rate of  $20$  mV s $^{-1}$ . The  $CrCl_3$  reaction also shows poor activity with very low current density. The reliable electrochemical properties of  $[Cr(CN)_6]^{4-/3-}$  are unique because of its low redox potential of  $-1.15$  V, which is lower than the potential of HERs in an aqueous system. The redox potential could arise from complexation effects, leading to the stabilization of the energy level of  $t_{2g}$  orbitals in the complex.<sup>[25]</sup> Simultaneously, controlling supporting electrolytes facilitate redox reactions with high stability and fast kinetics. Indubitably, side reactions associated with water splitting emerge as primary considerations in designing aqueous RFBs. In terms of thermodynamic conditions, the standard reduction potentials of the negolyte and the posolyte exhibit at  $-1.15$  and  $0.49$  V (versus SHE), respectively. Given the pH of each electrolyte, the HER ( $-0.8$  V versus SHE at pH 13) on the negolyte side presents more challenges than the oxygen evolution reaction (OER at  $0.8$  V versus SHE at pH 7) on the posolyte side. However, when taking the reaction kinetics into account, the redox system of  $[Cr(CN)_6]^{4-/3-}$  possesses simpler reaction pathways compared to HER. This is because it involves only a single electron, as opposed to two electrons, as seen in  $[Cr^{III}(CN)_6]^{3-} + e^- \rightarrow [Cr^{II}(CN)_6]^{4-}$  in the redox system and  $2H_2O + 2e^- \rightarrow H_2 + 2OH^-$  in the case of HER. It is well-known that single-electron reactions are generally preferable at high current densities from a kinetic standpoint rather than thermodynamics. To validate the plausible properties of  $[Cr(CN)_6]^{4-/3-}$ , various aspects influencing such formidable properties are needed to discuss in more detail in the next section.

The chemical stability that relies on long-term cycling should invariably be ensured due to the less stable Cr(II) complex that forms during redox reactions. The stability of metal complexes can be considered by the association constant (or stability constant,  $K_f$ ), which is the equilibrium constant for reactions forming metal complexes and indicates the strength of interactions between metal ions and ligands. The higher association constant means having stronger metal–ligand interactions and good thermodynamic stability.  $[Cr^{III}(CN)_6]^{3-}$  is thermodynamically stable and inert complex ( $K_f = 10^{33}$ ;  $K_f$  is the association constant of

the metal complex).<sup>[32]</sup> On the other hand,  $[Cr^{II}(CN)_6]^{4-}$ , which is the reductive form of the hexacyanochromate ions, has a lower  $K_f$  ( $10^{21}$ ) than that of  $[Cr(CN)_6]^{3-}$ . This means that  $[Cr(CN)_6]^{4-}$  is thermodynamically less stable and more labile, resulting in more easily undergoing ligand exchange processes substituting  $CN^-$  with  $H_2O$  or  $OH^-$  ligands, failure to maintain metal complex structure, and forming the insoluble chromium hydroxide ( $Cr(OH)_x$ ). This can be the dominant loss mechanism of active species during electrochemical reactions from  $[Cr^{III}(CN)_6]^{3-}$  to  $[Cr^{II}(CN)_6]^{4-}$ , and causes increasing irreversible capacity of the RFB. Furthermore, the parasitic HER at the charging process should be suppressed. This is because it increases the pH of the negolyte, accelerating unexpected ligand exchange by  $OH^-$  and the formation of  $Cr(OH)_x$ . Therefore, it is necessary to design an environment to mitigate these processes and improve the stability of hexacyanochromate ions during a repeated redox reaction.

Supporting electrolytes can open up new opportunities to suppress undesirable ligand exchanges and destruction of active materials, especially considering the less stable Cr(II) complex in  $[Cr(CN)_6]^{4-}$ . Also, high concentrations of supporting electrolytes can limit trace solubility, potentially extending the cathodic electrochemical stability window of water beyond the thermodynamic level of  $-0.8$  V versus SHE.<sup>[33]</sup> In addition, concentrated supporting electrolytes decrease the chemical activity of water, resulting in less ligand exchange to  $OH^-$ . As a cyanide-based supporting electrolyte, sodium cyanide (NaCN) was selected for the excellent electrochemical stability, especially against very reductive potentials, combined with a high solubility in water. Long-term CV data in Figure 2c,d compares the stability of  $[Cr(CN)_6]^{4-/3-}$  redox reactions in the cyanide-based supporting electrolyte (NaCN) to the NaCl supporting electrolyte. The initial cycles using both NaCl and NaCN supporting electrolytes in Figure 2c,d clearly show the reversible reduction and oxidation reactions near  $-1.2$  and  $-1.1$  V, respectively. Whereas the current density when using the NaCl electrolyte rapidly diminished and was rarely detected after 70 cycles, suggesting that the NaCl supporting electrolyte did not alleviate the ligand exchange and the redox species might result in forming  $Cr(OH)_x$  via side reactions; such material might be deposited on the glassy carbon electrode.<sup>[34]</sup> On the other hand, the current density and redox potentials using NaCN supporting electrolyte were maintained even after 1000 cycles as shown in Figure 2d, which was expected since the ligand exchange was limited by the number of cyanide ligands. Unlike the chloride based solutions, the excessive cyanide ions played a significant role in suppressing decomposition and maintaining a high stability of  $[Cr(CN)_6]^{4-/3-}$ . Additionally, a comparison of the initial solution and the solution aged for 10 days with  $5 \times 10^{-3}$  M  $K_3[Cr(CN)_6]$  via a CV curve and UV–visible spectra showed minimal damage to the materials properties after storage (Figure S2, Supporting Information). The minor degradation observed may primarily be due to exposure to the outside atmosphere during the repeated experimental process of sampling and conducting the CV test of the 10-day old solution. Under regular experimental conditions, where the solution is sealed, stability issues during solution storage may not be significant.

The fast kinetics of electrochemical reactions can be understood by analyzing associations between the CV scan rate and the corresponding current density as shown in Figure 2e,f. The

CV data, which were scanned from 5 to 500 mV s<sup>-1</sup>, show small potential shifts from 81 to 134 mV (Figure 2e and Table S1, Supporting Information) and exhibit high current densities during redox processes, even at the high scan rate of 500 mV s<sup>-1</sup>, indicative of a stable redox system with high charge and discharge conditions. The corresponding peak currents exhibit a linear relationship with respect to the square root of the scan rates as shown in Figure 2f. The small  $\Delta E_p$  is comparable with the value in the diffusion-controlled kinetic regime such that the slope in Figure 2f can thus be used to determine the diffusion coefficient ( $D_0$ ) via the Randles–Sevcik equation. Since the slopes of the cathodic and anodic processes are  $\pm 0.0002$ , the diffusion coefficient  $D_0$  is calculated as  $7.16 \times 10^{-6}$  cm<sup>2</sup> s<sup>-1</sup>. The charge transfer rate ( $k^0$ ) can also be calculated using the Nicholson method that provides the information about the relationship between  $\Delta E_p$  and  $k^0$  (Table S2, Supporting Information).<sup>[35]</sup> According to this method, the  $k_0$  is calculated as  $6.03 \times 10^{-3}$  cm s<sup>-1</sup>, facilitating that  $[\text{Cr}(\text{CN})_6]^{4-/3-}$  redox couples show the outstanding quasi-reversible behavior without any catalysts compared to other Cr-based materials.<sup>[23,26–28]</sup> Table S3 (Supporting Information) compares the electrochemical properties of the reduction potential, diffusion coefficient, and charge transfer rate in the hexacyanochromate complex with those obtained by previous studies. In particular,  $k^0$  of  $[\text{Cr}(\text{CN})_6]^{4-/3-}$  redox couple is approximately 6000 times higher than Cr<sup>II/III</sup> redox couple in CrCl<sub>3</sub> without catalysts and even six times higher than that with Bi catalyst. Additionally, it is higher than that of Cr<sup>II/III</sup>-PDTA redox couple ( $1.7 \times 10^{-4}$  cm s<sup>-1</sup>), which had previously been considered to have the best performance among Cr-based systems. Our electrochemical analyses of the  $[\text{Cr}(\text{CN})_6]^{4-/3-}$  complex indicate that it exhibits desirable behavior that enables fast kinetics with high stability at low redox potentials below the HER, which can be a promising candidate as a negolyte for sustainable RFB systems.

## 2.2. Theoretical Consideration by DFT Simulation of Chromium-Based Compounds

We performed molecular simulations to understand the complex chemistry behind the stable redox reaction of the  $[\text{Cr}(\text{CN})_6]^{4-/3-}$  coordination compound at low potential. Although it is already well-known concept that Cr(CN)<sub>6</sub> has the low-spin state of *d*-electrons, the theoretical analysis was carried out to investigate how the spin state can affect the properties compared to various chromium octahedral complexes with other ligands.<sup>[36]</sup>

By calculating the electronic structures and redox reaction energies of various Cr<sup>II</sup>-ligand complexes using DFT, we revealed the complex interplay between ligands and electronic structure in governing redox potential. Since frontier molecular orbitals (MOs), including the highest occupied and lowest unoccupied MOs, are important for the redox behaviors of coordination compounds, we compared electronic configurations of the frontier MOs of representative Cr<sup>II</sup>-based compounds using DFT calculation as presented in Figure 3a. We considered triplet ( $t_{2g}^4$ ) and quintet ( $t_{2g}^3 e_g^1$ ) states for each Cr<sup>II</sup>-based compound in order to find the energetic stable spin states (Table S4, Supporting Information).  $[\text{CrCl}_6]^{4-}$ ,  $[\text{Cr}(\text{H}_2\text{O})_6]^{2+}$ ,  $[\text{Cr}(\text{NH}_3)_6]^{2+}$ , and  $[\text{Cr-PDTA}]^{2-}$  are stable in their quintet states (high-spin state), whereas  $[\text{Cr}(\text{CN})_6]^{4-}$  is stable in its triplet states (low-spin state);

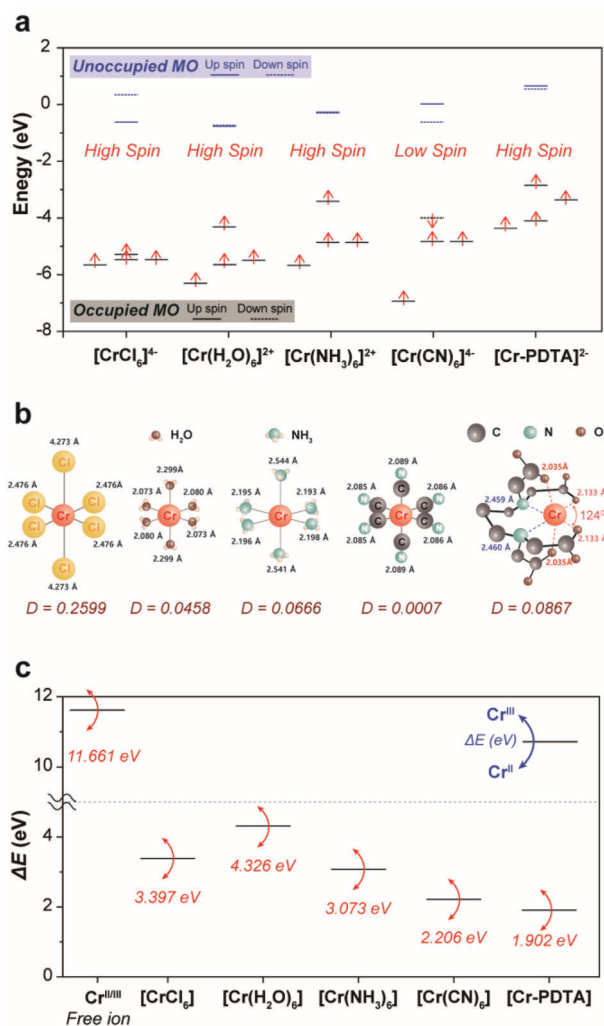


**Figure 3.** Simulated electronic configurations, Jahn–Teller distortions, and redox reaction energies of Cr<sup>II</sup>-based compounds. a) Energy levels of electronic orbitals. The upward arrows represent electrons with up-spin, and the downward arrows represent electrons with down-spin. Black solid and dashed lines denote occupied molecular orbitals (MOs) for up-spin and down-spin, respectively. Blue solid and dashed lines indicate unoccupied MOs for up-spin and down-spin, respectively. b) Molecular structures with bond lengths of ligands and distortion index *D* of octahedral complex. c) Calculated energy changes during Cr<sup>II/III</sup> redox reactions in these compounds.

these findings are consistent with conventional understanding that strong-field ligands such as CN<sup>-</sup> result in low-spin states due to their large *d* orbital splitting.

Since the Cr<sup>II</sup>-based compounds with high-spin state have single electron at  $e_g$  states, thereby leading to strong Jahn–Teller distortions, bonds with two ligands along *z* direction are more elongated than the bonds with other four, as shown in Figure 3b. In contrast,  $[\text{Cr}(\text{CN})_6]^{4-}$  has weak Jahn–Teller distortions due to unevenly occupied  $t_{2g}$  orbitals in the low-spin state, allowing for negligible elongation of bonds along the *z* direction.

To compare distortion degree, we calculated the distortion index using the following equation:

$$d = \frac{1}{n} \sum_{i=1}^n \frac{|l_i - l_{av}|}{l_{av}} \quad (1)$$

where  $l_i$  is the distance from the central Cr atom to the  $i^{\text{th}}$  ligand and  $l_{av}$  is the average distance. The strength of Jahn–Teller distortion (i.e., the degree of distortion) when transitioning to a Cr<sup>II</sup> state is intrinsically related to the kinetics of the Cr<sup>II/III</sup> redox reaction. The kinetics of electrochemical reactions are usually defined by the reorganization energy, which is initially introduced by Marcus,<sup>[37]</sup> the required energy for the rearrangement of the ligand and solvent between the initial and final states during charge transfer reactions. The Jahn–Teller distortion significantly affects this reorganization energy that a weak Jahn–Teller distortion caused by the low-spin state of the  $d_4$  configuration during redox reactions often correlates with a smaller reorganization energy, resulting in fast redox kinetics.<sup>[38]</sup> [CrCl<sub>6</sub>]<sup>4−</sup> has a larger distortion index of 0.2599 than others with a high-spin state because of its negatively charged ligands, which is in agreement with strong stabilization of the highest occupied  $e_g$  state in Figure 3a. [Cr(CN)<sub>6</sub>]<sup>4−</sup> has the smallest distortion index of 0.007 due to weak Jahn–Teller effects. It is thus inferred that the fast kinetics of the [Cr(CN)<sub>6</sub>]<sup>4−</sup> negolyte is mainly attributed to its facile redox reaction with weak Jahn–Teller distortion. We further calculated energy changes in these compounds during Cr<sup>II/III</sup> redox reactions. As shown in Figure 3c, [Cr(CN)<sub>6</sub>]<sup>4−</sup> exhibits significantly smaller energy changes compared to other compounds except [Cr-PDTA]<sup>2−</sup>, explaining its low potential observed in our experimental results (Figure 2a). Another Cr-complex with low energy change, [Cr-PDTA]<sup>2−</sup>, corresponds to the reported value of a low reduction potential (−1.11 V versus SHE),<sup>[17]</sup> despite forming a high-spin state. Although the compound of [Cr-PDTA]<sup>2−</sup> is encapsulated by steric ligands, its redox kinetics are relatively slower than the low-spin [Cr(CN)<sub>6</sub>]<sup>4−</sup> due to a relatively higher distortion index. Our DFT calculations show that the coordination compound of [Cr(CN)<sub>6</sub>]<sup>4−/3−</sup> possesses stable and fast redox reactions at a low potential of −1.15 V, which is enabled by the low-spin configuration of Cr<sup>II</sup>.

### 2.3. Full Redox Flow Battery Using Hexacyanometallates

After carefully validating the desirable properties, we built a full RFB cell composed of [Cr(CN)<sub>6</sub>]<sup>4−/3−</sup> and [Fe(CN)<sub>6</sub>]<sup>4−/3−</sup> redox couples as shown in Figure 1a and Figure S3 (Supporting Information). The preliminary half-cell data in Figure 2a suggest that the standard thermodynamic potential of the two negolyte and posolyte is 1.64 V. However, it is notorious that a half-cell CV test does not always correlate to full-cell data measured in a constant current mode because the potential-derived characterization is imprecise due to the overlapped faradaic response for the forward process, especially in the potential regime below HER. In this regard, we have verified the galvanostatic profile for the full-cell configuration, showing a highly reversible capacity of 10.2 Ah L<sup>−1</sup> at a discharging current density of 50 mA cm<sup>−2</sup> with an average potential of 1.43 V (Figure 4a). In particular, the redox mediators of [Cr(CN)<sub>6</sub>]<sup>4−/3−</sup> are coordination compounds

that are well known to exhibit vivid colors depending on the  $d$  orbital energy gap of transition metals. During the discharge process, the color of the negolyte in Figure 4a changes from dark brown to light red, as also shown in Movie S1 (Supporting Information). The UV–Vis spectra depending on the state of charge (SOC), shown in Figure 4b, also reveals corresponding species such that the peak at 326 nm indicates the charged state of [Cr(CN)<sub>6</sub>]<sup>4−</sup>.<sup>[39–41]</sup> As the color changes to light red, the correlated peaks at 307 and 377 nm increase together with increased concentrations of [Cr(CN)<sub>6</sub>]<sup>3−</sup>, implying that comprehensive redox change occurred in the full-cell configuration with excellent reductive stability. Another post-mortem XRD analysis also manifests successful conversion to [Cr(CN)<sub>6</sub>]<sup>4−</sup> as shown in Figure 4c. We used dried powder obtained by evaporating solvent of the negolyte at the different SOC of 0%, 50%, and 100%. Asterisks (\*) in Figure 4c indicate the information of NaCN reference, which was exploited to calibrate peak positions across different samples. The enlarged XRD patterns at 32°–35° in Figure 4c clearly elucidate that the dried samples show good agreement with the conventional K<sub>3</sub>[Cr(CN)<sub>6</sub>] and K<sub>4</sub>[Cr(CN)<sub>6</sub>] phases upon the SOC, implying a successful phase transition from [Cr(CN)<sub>6</sub>]<sup>4−</sup> to [Cr(CN)<sub>6</sub>]<sup>3−</sup>.

Cell polarization curves and power densities in Figure 4d,e enable to the fast kinetics of [Cr(CN)<sub>6</sub>]<sup>4−/3−</sup> to be deduced for the full-cell configuration. This advance allows accurate demonstration of the electrochemical behavior of [Cr(CN)<sub>6</sub>]<sup>4−/3−</sup> as well as the implementation of hexacyanometallates for a genuine energy storage application with competitive performance. Using our characterization of the current-voltage behavior at various SOC values (0%, 10%, 25%, 75%, and 100%), we achieved a remarkable performance of [Cr(CN)<sub>6</sub>]<sup>4−/3−</sup> even without using any catalysts, such as bismuth, titanium, or a porous current collector.<sup>[12,42–44]</sup> Open-circuit voltage (OCV) and ohmic resistance were obtained from Figure S4a (Supporting Information). The OCV increased from 1.55 to 1.80 V. The linear ohmic region of SOC 50%, between 1.25 and 1.5 V, shows an area-specific resistance (ASR) of 1.82 Ω. The OCV increased from 1.55 to 1.80 V with increasing the SOC (Figure S4b, Supporting Information). The thermodynamic full-cell voltage obtained by the OCV of SOC 50% was 1.63 V, similar to the theoretical cell voltage derived by the standard reduction potential of active materials of each side, as shown in Figure 2a. The linear ohmic region of SOC 50%, between 1.25 and 1.5 V, suggests that the redox reaction is not the main factor determining the cell performance. The calculated ASR from the ohmic region is 1.82 Ω, which is determined mainly by cell components. Furthermore, the maximum peak power density reaches 410 mW cm<sup>−2</sup> as shown in Figure 4d, denoting that the material is a promising candidate for large-scale energy storage field. The rate performance test at the different current densities demonstrates that our flow cell can operate within a range from 20 to 150 mA cm<sup>−2</sup>, as shown in Figure S5 (Supporting Information). The energy efficiency of the cell remains approximately 80% or higher up until a density of 100 mA cm<sup>−2</sup>, and close to 70% at 150 mA cm<sup>−2</sup>. The Coulombic efficiency exceeded 97% at current densities above 50 mA cm<sup>−2</sup> and reached 99% at 100 and 150 mA cm<sup>−2</sup>. However, the relatively low Coulombic efficiency at lower current densities (20 and 30 mA cm<sup>−2</sup>), which is under 95%, can be attributed to the increased activity of the HER at these low current

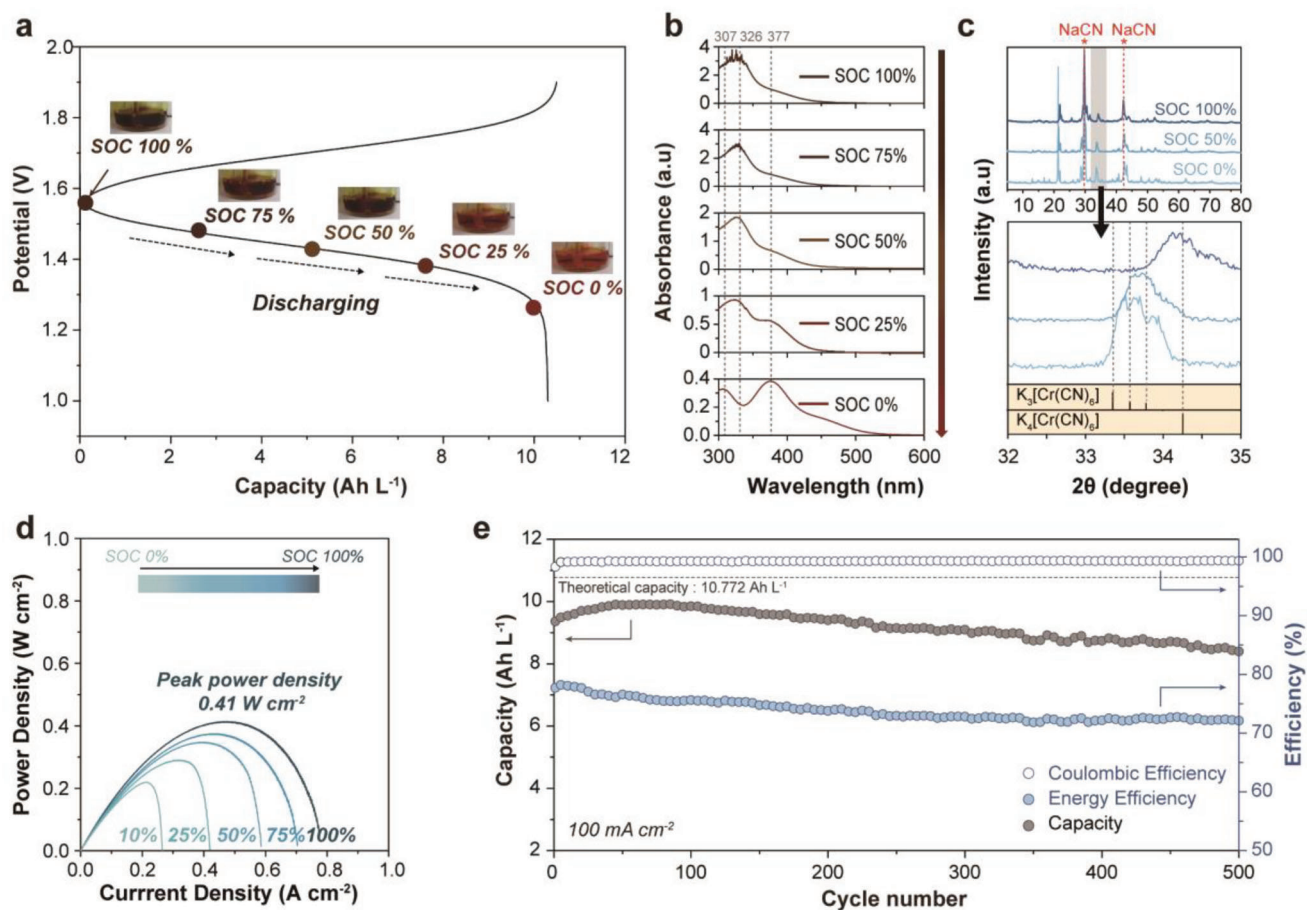


**Figure 4.** Full-cell performance of 0.4 M  $K_3[Cr(CN)_6]$ . a) A typical voltage profile of  $K_3[Cr(CN)_6]$  and the corresponding solution images at different states of SOC (0%, 25%, 50%, 75%, and 100%). b) UV-Vis spectra of  $K_3[Cr(CN)_6]$  at different states of SOC (0%, 25%, 50%, 75%, and 100%). The single peak at 326 nm indicates the charged state of  $[Cr(CN)_6]^{4-}$  and the peaks at 307 and 377 nm denote the discharged state of  $[Cr(CN)_6]^{3-}$ . c) XRD data of the post-mortem dried samples at SOC of 0%, 50%, and 100%. d) Power density as a function of the current density at the different states of SOC (0%, 25%, 50%, 75%, and 100%). e) Plots of the Coulombic efficiency, energy efficiency, and capacity for 500 cycles ( $\pm 100 \text{ mA cm}^{-2}$ ). A total of 30 mL of 0.4 M  $K_3[Cr(CN)_6]$  solution was used as a negolyte with 2.5 M NaCN as a supporting electrolyte. As a posolyte, 40 mL of 0.4 M  $K_4[Fe(CN)_6]$  was dissolved in 2.5 M NaCl supporting electrolyte. The data was represented at intervals of every five cycles.

densities, implying that a very low charging rate can be detrimental to our battery system, when the redox reactions occur under HER.

This charge transfer kinetics in the full-cell configuration does not seem to limit power output, which is in good agreement with the rapid kinetics presented in Figure 2e,f. Long-term cycling performance of  $[Cr(CN)_6]^{4-/3-}$  and  $[Fe(CN)_6]^{4-/3-}$  complexes at a current density of  $100 \text{ mA cm}^{-2}$  (Figure 4f and Figure S4c,d, Supporting Information) shows high Coulombic efficiency, energy efficiency, and normalized capacity for 500 cycles. The Coulombic efficiency is another vital factor for evaluating the electrochemical performance of hexacyanometallates because it determines the reversibility of the redox processes and the inactivity of HER. Promising averaged Coulombic efficiencies of 99.29% were achieved for 500 cycles, inferring the truly reversible reaction of redox mediators. The energy efficiency was also maintained above 70% (average 73.85% for 500 cycles), because of the overpotential between charge and discharge at the high current density. The capacity decay was calculated to be less than

0.02% per cycle, denoting that there are no significant side reactions such as the fatal decomposition of active materials or HER.

For long-lasting cycling, possible degradation might occur at the posolyte and negolyte. Cycling tests on degraded flow cells mainly exhibited capacity fading at the posolyte. For example, when an extra posolyte of  $K_4[Fe(CN)_6]$  was added after 1100 cycles in a slightly degraded flow cell, the diminished capacity recovered immediately to the initial cycle, as shown in Figure S6 (Supporting Information), suggesting that the gradual capacity fading occurred due to the consumption of counter posolytes. As far as the compatibility issues are concerned, this hexacyanometallate configuration of both posolyte and negolyte is recommended considering the validity of the specifically nonparametrized full cells of kinetic parameters of the two reaction rates, lifespans, redox flow mediators, and flowing flux. If both electrodes have different redox reactions, such as single- or two-electron redox reactions, it is difficult to match the rate capability and cyclability of both electrolytes.

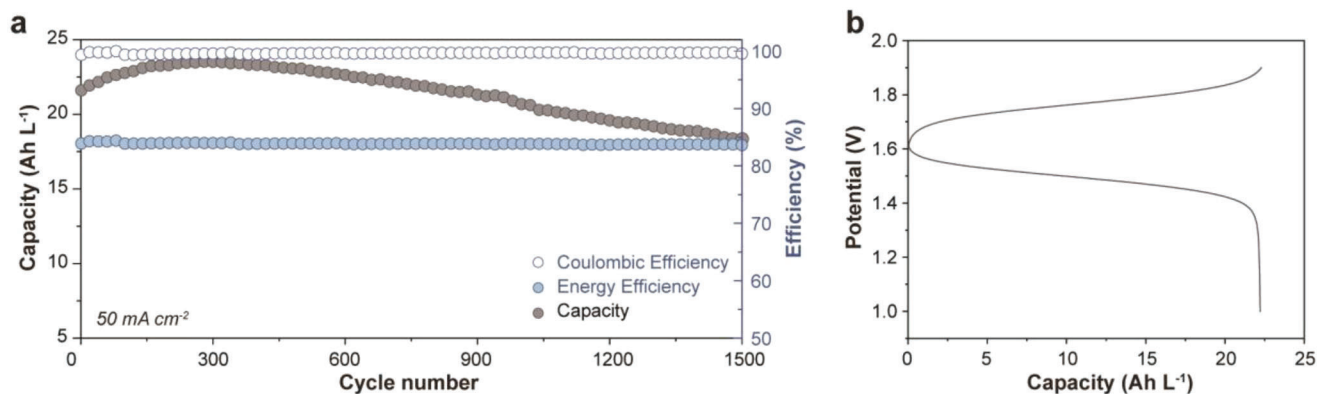


**Figure 5.** Stability test of 1 M  $\text{K}_3[\text{Cr}(\text{CN})_6]$  with excessive posolyte. a) Cycling profiles of discharge capacity, Coulombic efficiency, and energy efficiency for 1500 cycles ( $\pm 50 \text{ mA cm}^{-2}$ ). A 1 M  $\text{K}_3[\text{Cr}(\text{CN})_6]$  solution was used as a negolyte with 2.5 M NaCN as a supporting electrolyte. A total of 50 mL of 0.35 M  $\text{K}_4[\text{Fe}(\text{CN})_6]$  and 0.1 M  $\text{K}_3[\text{Fe}(\text{CN})_6]$  with 2.5 M NaCl was used as a counter posolyte. The data was represented at intervals of every 20 cycles. b) A typical voltage profile corresponded to (a).

We also validated the utilization of the full-cell at a higher negolyte concentration of 1 M, which is close to the maximum solubility of  $\text{K}_3[\text{Cr}(\text{CN})_6]$ . Considering the solubility of  $\text{K}_3[\text{Cr}(\text{CN})_6]$  per se, up to 1.1 M can be dissolved in water with 2 M NaCN supporting electrolytes. The solubility in water with 2 M NaCN supporting electrolyte was measured by fitting the UV-Vis spectra, as shown in Figure S7 (Supporting Information). The peak intensity of the fully saturated solution was 1.28014 at 432 nm. Using the high solubility in aqueous media, we employed full-cell tests with 1 M concentrated  $\text{K}_3[\text{Cr}(\text{CN})_6]$  with the different amount of the posolytes (Figure 5 and Figure S8, Supporting Information). When 1 M concentrated  $\text{K}_3[\text{Cr}(\text{CN})_6]$  was operated with excessive amount of the posolyte, the cell exhibited stable cyclability for 1500 cycles, as shown in Figure 5, suggesting that the cycle life is strongly dependent on the charge balance during cell operation.

Although the full-cell system showed outstanding performance, especially for the negolyte part, additional studies to find other proper posolyte are needed for more advanced performances. In the current system, the low solubility of the full-cell in Figure 4 was determined by the limited solubility of the posolyte,  $\text{K}_4[\text{Fe}(\text{CN})_6]$ , which is less than 0.4 M. If the counter species is used, the critical obstacle could be overcome to improve the cell performance, particularly under the high-concentration condition. First, this solubility compatibility causes concentration mismatch at high-concentration  $\text{Cr}(\text{CN})_6$ , resulting in water-molecule migration due to osmotic pressure. Based on this problem, it is difficult to design a proper  $\text{Cr}(\text{CN})_6$  negolyte, such as tuning the concentration of active materials and supporting electrolytes. Furthermore, the utilized volume of the posolyte should be increased when using a high-concentration negolyte, decreasing the volumetric energy density of the system. The total volume of the negolyte and posolyte should be considered in practical cell operation. The volumetric energy density determined by both side electrolytes is crucial. The large amount of the posolyte increases the entire volume of electrolyte and decreases the energy density of the battery system. This can become a critical disadvantage when setting the system in a practical situation.

Figure S8a (Supporting Information) shows that galvanostatic charging-discharging profiles of a 1 M full-cell at the 1<sup>st</sup>

and 5<sup>th</sup> cycles have identical plots as discharge capacities of 531.76 and 531.03 mAh, respectively, suggesting that this system can utilize 99% of the theoretical capacity even at the near-maximum concentration. This full-cell could achieve an energy density of 38.6 Wh L<sup>-1</sup>, an outstanding value compared to common aqueous RFBs, such as all-vanadium flow batteries of 16–33 Wh L<sup>-1</sup>.<sup>[45]</sup> With compatible matching between the  $\text{K}_4\text{Fe}(\text{CN})_6$  posolyte and  $\text{K}_3\text{Cr}(\text{CN})_6$  negolyte as a whole energy-density wise, the high-concentration full-cell exhibited 80% capacity retention for 80 cycles as shown in Figure S8b,c, Supporting Information. Because the low solubility of  $[\text{K}_4\text{Fe}(\text{CN})_6]$  (<0.4 M) caused the concentration mismatch with 1 M  $[\text{K}_3\text{Cr}(\text{CN})_6]$ , resulting in water-molecule migration due to osmotic pressure. In addition, the limited solubility of the counter species becomes a critical obstacle to designing appropriate hexacyanochromate-based negolytes, such as tuning the concentration of supporting electrolytes. These can influence cell operations and must be more seriously considered for long-term operation at a high-concentration. As a plausible clue for limited concentration, Wu et al. reported that the solubility of ferrocyanide could increase to 1.5 M by cation exchange to ammonium ions, enhancing the long-term stability and performance of RFBs at high concentrations.<sup>[41]</sup> In this regard, to achieve high energy density as a full-cell configuration, the compatible energy density, solubility, and reaction kinetics of posolytes and their well-matched counterparts are in strong demand.

### 3. Discussion

For a complete assessment of the study materials for practical applications, we have to consider the significant degradation mechanisms of RFBs, such as cross-over, self-decomposition of active materials, and electrolyte side reaction.<sup>[46]</sup> Cross-overs denote the ion-transport of active electrolytes across ion-conducting membranes leading to undesirable migration of ions in posolytes, negolytes, and/or supporting electrolytes. In this work, we employed a cation-exchanged Nafion membrane that transports mobile cations and excludes the negatively charged anions either by size or Donnan exclusion effects (Figure 1a). Since

$[\text{Cr}(\text{CN})_6]^{4-/3-}$  and  $[\text{Fe}(\text{CN})_6]^{4-/3-}$  hexacyanometallates are surrounded by strong-field ligands of cyanides, the outer region of the octahedral redox species is strongly negative, resulting in complete exclusion dominated by electrostatic interactions within the membrane. Bakajin et al. measured ion exclusion coefficients using the Donnan model, suggesting that  $\text{K}_3\text{Fe}(\text{CN})_6$  showed near-complete exclusion due to its high cation-anion valence (1/3), which indicates high electrostatic repulsion.<sup>[47]</sup> The self-decomposition of active materials and electrolyte side reactions should also be considered for stable RFBs since the chemical decomposition of redox species causes deterioration of the intrinsic property of active materials.  $[\text{Fe}(\text{CN})_6]^{4-/3-}$  is widely used as a reference posolyte due to its highly stable performance without compromising the self-decomposition of active materials. In the case of  $[\text{Cr}(\text{CN})_6]^{4-/3-}$ , we observed that the charged state of  $[\text{Cr}(\text{CN})_6]^{4-}$  tends to partially exchange cyanide with hydroxyl ( $\text{OH}^-$ ) ligands via photoaquation mechanism, which is well-known in metal complexes (Figure S9a, Supporting Information).<sup>[41–43]</sup> It is also known that the photoexcitation of the hexacyanometallates might lead either to its dissociation into  $\text{CN}^-$  and  $[\text{Cr}(\text{CN})_5]^{3-}$  fragments or the formation of  $[\text{Cr}(\text{CN})_5(\text{H}_2\text{O})]^{3-}$  in a general aqueous medium.<sup>[41,48]</sup> However, cyanide complexes tend to show different features depending on the solvent interaction, thereby influencing the electronic structure. A feasible mechanism of ligand stability in this system is that the cyanide-based supporting electrolyte can offer an opportunity to control the condition of the aqueous solvent. As shown in Figure S9b (Supporting Information), although as-synthesized  $\text{K}_3\text{Cr}(\text{CN})_6$  is coordinated with aqua ligands observed in UV–Vis spectra, the subsequent complex after first cycle verifies ligand exchange to cyanides forming  $\text{K}_3\text{Cr}(\text{CN})_6$ .<sup>[40,41]</sup> Our results provide clear examples both of the energy dependence of ligand exchanges and of the role of supporting electrolytes in the reactivity of metal complexes. We therefore conclude that by harnessing this advantage, the suggested RFB system can operate the prolonged cycles without cross-over problems and chemical decomposition, including ligand exchange. The safety of free cyanides (hydrogen cyanide (HCN) and cyanide ions ( $\text{CN}^-$ )) needs to be discussed. In particular, gaseous HCN is very hazardous to people. Gaseous HCN molecules can easily spread into the air and become an inhalation risk. Problematic HCN is dominant at low pH, as the pKa of HCN is 9.2; 99% of free cyanides exist in the form of HCN below pH 7.<sup>[49]</sup> However, most of the free cyanides in the present system exist in the form of  $\text{CN}^-$  in the electrolyte solution because the operating pH of the electrolytes is 13–14. More than 99.99% of free cyanides exist as  $\text{CN}^-$  anions in solution at this pH range (Figure S10, Supporting Information). Of course, extreme care is needed when handling cyanide ions and ensuring that the redox flow systems are indeed under the safety regulation.

Although hexacyanometalate-based RFBs have shown promising electrochemical performances against the aforementioned issues, some unexpected degradation, such as leakage of electrolytes and precipitation as salts, may occur in the system, thereby facilitating the replacement or rebalancing the ratio of the active material solutions while maintaining the infra-tank and pump systems.<sup>[50]</sup> To evaluate conceptual and technological potential, we prepared an intentionally degraded negolyte and replaced it with a new  $\text{K}_3[\text{Cr}(\text{CN})_6]$  solution as shown in Figure S11

(Supporting Information). Following the replacement, the specific capacity reaches the original performance after a couple of cycles for aging processes that are required to match the counterpart capacity with the posolyte.

The outstanding properties of hexacyanometallates are not only limited to RFBs, possible exploring their application in a variety of ambitious projects. The main advantage of the  $[\text{Cr}(\text{CN})_6]^{4-/3-}$  redox system is the very low redox potential of the negolyte due to the coordination with strong-field ligands retaining high stability even against HER. A comparison against other well-known aqueous RFB systems (Figure 6) shows that this high overall potential is contributed by the potential of the negolyte,  $[\text{Cr}(\text{CN})_6]^{4-/3-}$ , suggesting a higher overall potential matching with high redox posolytes. We note that the low redox potential of  $[\text{Cr}(\text{CN})_6]^{4-/3-}$  will benefit from knowledge obtained by other electrochemical technologies, such as  $\text{CO}_2$  electroreduction processes and biomass conversion.<sup>[51]</sup> Therefore, we believe that this invention will contribute significantly to stationary energy storage in other areas that prefer to combine with continuous-flow electroreduction systems.

## 4. Conclusion

In the quest for sustainable RFBs, we have discovered the new negolyte,  $\text{K}_3[\text{Cr}(\text{CN})_6]$ , which exhibits a low redox potential of  $-1.15$  V versus SHE, stable cycling performance, and fast charge transfer kinetics. The coordination with strong-field ligands observed herein is expected to play important roles in governing the low-spin state of  $\text{Cr}^{\text{II}}$ , thereby allowing low redox potential during electrochemical cycling. On the basis of a wide variety of RFB chemistries beyond hexacyanometallates, our results, coupled with high stability and fast kinetics, will help to guide the development of RFBs with high-energy densities and prolonged lifetimes. Our thermodynamic DFT calculation also confirms that the cyanide-coordinated molecules can promote the fast kinetics attributed by virtue of their facile redox reaction via weak Jahn–Teller effects rather than the strong Jahn–Teller effects characterizing other compounds. The prototype full-cell configuration highlights a stable lifetime to 500 cycles, and a high-energy density of  $38.6$  Wh  $\text{L}^{-1}$ , surpassing the difficulties of vanadium RFB. In comparison to conventional and other flow batteries, this cell configuration has superior properties in terms of the full-cell potential and cycling performance. Consequently, we believe that our new proposed  $[\text{Cr}(\text{CN})_6]^{4-/3-}$  systems represents a novel and scientifically intriguing material that can push forward the development of grid energy storage.

## 5. Experimental Section

*Synthesis of Potassium Hexacyanochromate ( $\text{K}_3[\text{Cr}(\text{CN})_6]$ ):*  $\text{K}_3[\text{Cr}(\text{CN})_6]$  was synthesized following a modified method based on previous literature.<sup>[52,53]</sup>  $\text{Cr}(\text{CH}_3\text{COO})_3$  (JUNSEI, Cr 21–25%) was dissolved in 20 mL distilled (DI) water and this solution was transferred into a boiling KCN (Alfa Aesar, 96.0%) solution (8.93 g of KCN in 30 mL DI water). 0.24 g of activated charcoal was added during the reaction, acting as a catalyst to promote the formation of  $\text{K}_3[\text{Cr}(\text{CN})_6]$  from the precursors. The chemical reaction for the formation of  $\text{K}_3[\text{Cr}(\text{CN})_6]$  is as follows:



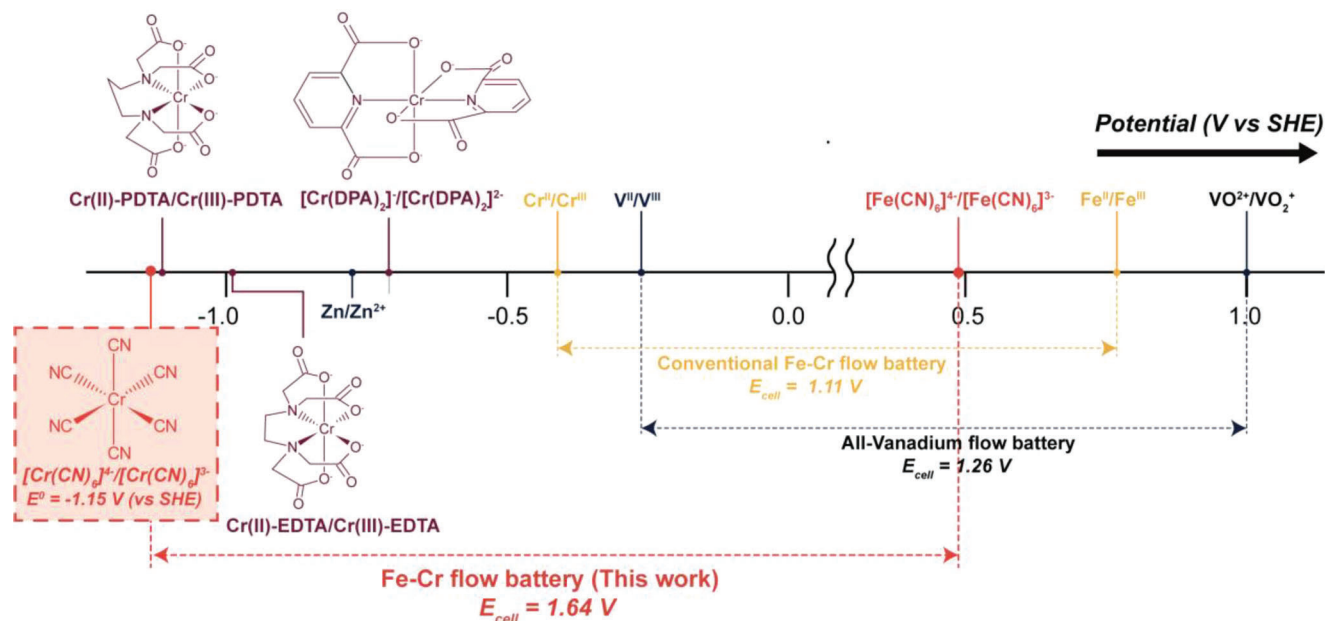


**Figure 6.** Standard redox potentials of aqueous redox flow batteries. All-vanadium systems possess relatively high potential region; this work covers the low redox potential of  $-1.15$  V versus SHE, which opens new avenues for the design of high-energy density RFBs.

After allowing all the ingredients to mix for 5 min, the activated charcoal was filtered and the filtered solution was partially dried in order to evaporate the remnant solvent. Finally, the solution was chilled to precipitate  $K_3[Cr(CN)_6]$  taking advantage of the solubility differences depending on temperature. This precipitated  $K_3[Cr(CN)_6]$  was filtered and washed by ethanol five times, then dried in a vacuum oven at  $40^\circ\text{C}$ . The synthesized  $K_3[Cr(CN)_6]$  was characterized by XRD and compare with commercial  $K_3[Cr(CN)_6]$  (Sigma–Aldrich, 99.99%).

**Half-Cell Characterization:** CV measurements were conducted using an EC-Lab potentiostat (BioLogic). A three-electrode system was employed with an Ag/AgCl reference electrode filled with a 3 M KCl solution, Pt wire as a counter electrode, and a 3 mm diameter-glassy carbon working electrode. A half-cell test was performed using the  $5 \times 10^{-3}$  and 0.1 M solutions containing synthesized  $K_3[Cr(CN)_6]$  with 1 M supporting electrolytes. To compare the redox reaction of chromium, experiments were conducted using the  $CrCl_3$  redox system as a reference. A total of  $5 \times 10^{-3}$  M  $CrCl_3$  (Sigma–Aldrich,  $\geq 98.0\%$ ) was dissolved in DI water with the supporting electrolyte of 1 M HCl.

**Flow Cell (Full-Cell) Characterization:** The full-cell test was conducted at the two different  $K_3[Cr(CN)_6]$  concentrations (0.4 and 1 M). The ratio of negolyte and posolyte active species was set to 1:1.3. A 0.4 M cell consisting of 30 mL of a 0.4 M  $K_3[Cr(CN)_6]$  solution with a 2.5 M NaCN (Alfa Aesar, 95%) as the supporting electrolyte, and 40 mL of a 0.4 M  $K_4[Fe(CN)_6] \cdot 3H_2O$  solution (Sigma–Aldrich, 98.5–102.0%) with 2.5 M NaCl (Alfa Aesar, 99.0%) supporting electrolyte. In the case of a 1 M cell, 20 mL of a 1 M  $K_3[Cr(CN)_6]$  solution with 3 M NaCN and 75 mL of a 0.35 M  $K_4[Fe(CN)_6] \cdot 3H_2O$  solution with 3 M NaCl were used. For the stability test at 1 M with highly excessive posolyte, 1 mL of 1 M  $K_3[Cr(CN)_6]$  solution with 2.5 M NaCN, and 50 mL of 0.35 M  $K_4[Fe(CN)_6] \cdot 3H_2O$  and 0.1 M  $K_3[Fe(CN)_6]$  (Sigma–Aldrich,  $> 99.0\%$ ) solution with 2.5 M NaCl were utilized. The flow battery cell (TS CHEM) was assembled with  $5\text{ cm}^2$  ( $2\text{ cm} \times 2.5\text{ cm}$ ) carbon-felt electrode (XF-30a, TOYOBO), graphite plate, copper current collector, and Nafion membrane. Nafion (NRE-212, Sigma–Aldrich, Nafion perfluorinated membrane, thickness 0.002 inch) was soaked in a 0.1 M HCl solution for 30 min then rinsed in DI water. The carbon felt electrode was heated to  $500^\circ\text{C}$  for 5 h under an air atmosphere. The anolytes and catholytes were circulated in a tube (Masterflex Norprene tubing, I.D. 3.18 mm, O.D. 6.35 mm) by pump drives (JenieWell,

JWSE600) at an average flow rate of approximately  $40\text{ mL min}^{-1}$ , where all carbon felt electrodes was compressed by  $\approx 70\%$  in a stack cell.

A galvanostatic charge–discharge test was performed using an EC-Lab potentiostat at room temperature. Before taking measurements, both the anolyte and catholyte were circulated for 2 h without applying a bias. A constant current was applied during the charging and discharging processes ( $100\text{ mA cm}^{-2}$ ) for a voltage cutoff range from 1 to 1.9 V. Power tests were conducted by potentiostat (IviumStat) at each SOC. Current scanning was employed during the discharging state in order to obtain peak power densities, which the cell was charged at a constant current density of  $30\text{ mA cm}^{-2}$ .

The state of the anolyte during full-cell operation was investigated using UV–Vis spectroscopy. The cell was charged at  $30\text{ mA cm}^{-2}$  and discharged at  $50\text{ mA cm}^{-2}$  from 1.0 to 1.9 V. An amount of 0.2 mL of the solution was extracted at each SOC (0%, 25%, 50%, 75%, and 100%,) and diluted them 1/100 times (0.004 M).

**Computational Details:** All first-principles calculations were conducted according to spin-unrestricted DFT using the Gaussian 09 package.<sup>[54]</sup> Geometry optimizations and MO energy level calculations were carried out following Becke–Lee–Yang–Parr (B3LYP) hybrid functional<sup>[55]</sup> and the 6–31G basis set. The solvation effect of water was modeled using the integral equation formalism polarizable continuum model (IEFPCM). Various spin states from singlet to septet were considered and the state with the lowest DFT energy was selected for each molecule.

**Solubility Test:** Various concentrations of  $K_3[Cr(CN)_6]$  solution were prepared (0.05, 0.1, 0.2, 0.3, 0.4 M, and unknown (saturated solution)). The unknown solution was made by adding  $K_3[Cr(CN)_6]$  into the 2 M NaCN solution until the solid could no longer be dissolved, after which the residue was filtered. The concentration of the unknown solution was evaluated using UV–visible spectroscopy. Absorbance is proportional to concentration. A precalibrated absorbance–concentration plot was obtained through the peak intensity at 429–432 nm for other solutions, and the solubility was calculated using this plot.

## Supporting Information

Supporting Information is available from the Wiley Online Library or from the author.

## Acknowledgements

This work was supported by the 2020 Research Fund (1.200115.01) of UNIST and Individual Basic Science & Engineering Research Program (RS-2023-00208929) through National Research Foundation of Korea funded by the Ministry of Science and ICT, and the Ministry of Trade, Industry & Energy/Korea Institute of Energy Technology Evaluation and Planning (MOTIE/KETEP) (20224000000390). The authors gratefully acknowledge the supercomputing resources of the UNIST Supercomputing Center. This study contains the results obtained by using the equipment of UNIST Central Research Facilities (UCRF).

## Conflict of Interest

The authors declare no conflict of interest.

## Author Contributions

J.J. and R.K. contributed equally to this work. J.J. and H.-W.L. conceived the idea, designed the experiments, and analyzed the data. J.J. and R.K. conducted all experiments with the assistance of S.J., C.L., J.Choi., Y.L., S.K., J.R., S.W.L., J.Cho., D.L., H.S., and W.C. D.-H.S. completed DFT simulations. J.J., R.K., D.-H.S., and H.-W.L. interpreted the results. J.J., D.-H.S., and H.-W.L. co-wrote the paper. All authors discussed the results and commented on the manuscript.

## Data Availability Statement

The data that support the findings of this study are available on request from the corresponding author. The data are not publicly available due to privacy or ethical restrictions.

## Keywords

fast kinetic redox species, hexacyanochromate, hexacyanometallates, redox-flow batteries, strong-field ligands, supporting electrolytes

Received: March 7, 2023

Revised: June 15, 2023

Published online: July 7, 2023

- [1] Z. Yang, J. Zhang, M. C. W. Kintner-Meyer, X. Lu, D. Choi, J. P. Lemmon, J. Liu, *Chem. Rev.* **2011**, *111*, 3577.
- [2] G. L. Soloveichik, *Chem. Rev.* **2015**, *115*, 11533.
- [3] P. Leung, X. Li, C. Ponce De León, L. Berlouis, C. T. J. Low, F. C. Walsh, *RSC Adv.* **2012**, *2*, 10125.
- [4] M. Park, J. Ryu, W. Wang, J. Cho, *Nat. Rev. Mater.* **2016**, *2*, 16080.
- [5] X. Li, P. Gao, Y. Y. Lai, J. D. Bazak, A. Hollas, H. Y. Lin, V. Murugesan, S. Zhang, C. F. Cheng, W. Y. Tung, Y. T. Lai, R. Feng, J. Wang, C. L. Wang, W. Wang, Y. Zhu, *Nat. Energy* **2021**, *6*, 873.
- [6] F. R. Brushett, M. J. Aziz, K. E. Rodby, *ACS Energy Lett.* **2020**, *5*, 879.
- [7] L. F. Arenas, F. C. Walsh, C. P. de León, *Flow Batteries: From Fundamentals to Applications*, Vol. 1 (Eds: C. Roth, J. Noack, M. Skyllas-Kazacos), Wiley-VCH Verlag, Hoboken, NJ, USA **2023**.
- [8] Y. Yao, J. Lei, Y. Shi, F. Ai, Y. C. Lu, *Nat. Energy* **2021**, *6*, 582.
- [9] L. F. Arenas, C. Ponce de León, F. C. Walsh, *Curr. Opin. Electrochem.* **2019**, *16*, 117.
- [10] W. Wang, Q. Luo, B. Li, X. Wei, L. Li, Z. Yang, *Adv. Funct. Mater.* **2013**, *23*, 970.
- [11] A. Parasuraman, T. M. Lim, C. Menictas, M. Skyllas-Kazacos, *Electrochim. Acta* **2013**, *101*, 27.
- [12] H. R. Jiang, J. Sun, L. Wei, M. C. Wu, W. Shyy, T. S. Zhao, *Energy Storage Mater.* **2020**, *24*, 529.
- [13] LIVE Vanadium Price, News and Articles, <https://www.vanadiumprice.com>, **2020**.
- [14] Y. K. Zeng, T. S. Zhao, L. An, X. L. Zhou, L. Wei, *J. Power Sources* **2015**, *300*, 438.
- [15] K. Lin, Q. Chen, M. R. Gerhardt, L. Tong, S. B. Kim, L. Eisenach, A. W. Valle, D. Hardee, R. G. Gordon, M. J. Aziz, M. P. Marshak, *Science* **2015**, *349*, 1529.
- [16] K. Gong, F. Xu, J. B. Grunewald, X. Ma, Y. Zhao, S. Gu, Y. Yan, *ACS Energy Lett.* **2016**, *1*, 89.
- [17] B. H. Robb, J. M. Farrell, M. P. Marshak, *Joule* **2019**, *3*, 2503.
- [18] W. Ruan, J. Mao, S. Yang, C. Shi, G. Jia, Q. Chen, *Chem. Commun.* **2020**, *56*, 3171.
- [19] A. Hollas, X. Wei, V. Murugesan, Z. Nie, B. Li, D. Reed, J. Liu, V. Spenkle, W. Wang, *Nat. Energy* **2018**, *3*, 508.
- [20] R. Feng, X. Zhang, V. Murugesan, A. Hollas, Y. Chen, Y. Shao, E. Walter, N. P. N. Wellala, L. Yan, K. M. Rosso, W. Wang, *Science* **2021**, *372*, 836.
- [21] D. A. Johnson, M. A. Reid, *J. Electrochem. Soc.* **1985**, *132*, 1058.
- [22] A. Adin, A. G. Sykes, H. S. Gates, E. L. Kin, *J. Chem. Soc. A* **1966**, *80*, 1518.
- [23] Y. K. Zeng, T. S. Zhao, X. L. Zhou, L. Zeng, L. Wei, *Appl. Energy* **2016**, *182*, 204.
- [24] C. Yang, G. Nikiforidis, J. Y. Park, J. Choi, Y. Luo, L. Zhang, S. C. Wang, Y. T. Chan, J. Lim, Z. Hou, M. H. Baik, Y. Lee, H. R. Byon, *Adv. Energy Mater.* **2018**, *8*, 1702897.
- [25] V. Bhatt, *Essentials of Coordination Chemistry*, Elsevier, Amsterdam **2016**.
- [26] C.-H. Bae, E. P. L. Roberts, R. A. W. Dryfe, *Electrochim. Acta* **2002**, *48*, 279.
- [27] C. Bae, E. P. L. Roberts, M. H. Chakrabarti, M. Saleem, *Int. J. Green Energy* **2011**, *8*, 248.
- [28] S. E. Waters, B. H. Robb, M. P. Marshak, M. P. Marshak, *ACS Energy Lett.* **2020**, *5*, 1758.
- [29] J. Walsh, J. Earley, *Inorg. Chem.* **1964**, *3*, 343.
- [30] R. G. Wilkins, R. E. Yelin, *Inorg. Chem.* **1968**, *7*, 2667.
- [31] J. Goeltz, D. Amadeo, A. J. Esswein, T. D. Jarvi, E. R. King, S. Y. Reece, N. Tyagi, *US 2017/0352905 A1* **2017**.
- [32] A. Smith, M. M. Botz, T. Mudder, *Chemistry and Treatment of Cyanidation Wastes*, Mining Journal Books Limited, London **1991**, p. 373.
- [33] L. Suo, O. Borodin, T. Gao, M. Olguin, J. Ho, X. Fan, C. Luo, C. Wang, K. Xu, *Science* **2015**, *350*, 938.
- [34] D. N. Hume, I. M. Kolthoff, *J. Am. Chem. Soc.* **1943**, *65*, 1897.
- [35] R. S. Nicholson, *Anal. Chem.* **1965**, *37*, 1351.
- [36] J. P. Eaton, D. Nicholls, *Transition Met. Chem.* **1981**, *6*, 203.
- [37] R. A. Marcus, *J. Chem. Phys.* **1956**, *24*, 966.
- [38] X. Zhang, M. L. Lawson Daku, J. Zhang, K. Suarez-Alcantara, G. Jennings, C. A. Kurtz, S. E. Canton, *J. Phys. Chem. C* **2015**, *119*, 3312.
- [39] A. Chiang, A. W. Adamson, *J. Phys. Chem.* **1968**, *72*, 3827.
- [40] D. K. Wakefield, W. B. Schaap, D. K. Wakefield2, *Inorg. Chem.* **1968**, *8*, 512.
- [41] L. Jefčić, S. W. Feldberg, *J. Phys. Chem.* **1971**, *75*, 2381.
- [42] C. D. Wu, D. A. Scherson, E. B. Yeager, E. J. Calvo, *J. Electrochem. Soc.* **1986**, *133*, 2109.
- [43] T.-M. Tseng, R.-H. Huang, C.-Y. Huang, C.-C. Liu, K.-L. Hsueh, F.-S. Shieu, *J. Electrochem. Soc.* **2014**, *161*, A1132.
- [44] X. L. Zhou, Y. K. Zeng, X. B. Zhu, L. Wei, T. S. Zhao, *J. Power Sources* **2016**, *325*, 329.

- [45] L. da Silva Lima, M. Quartier, A. Buchmayr, D. Sanjuan-Delmás, H. Laget, D. Corbisier, J. Mertens, J. Dewulf, *Sustainable Energy Technol. Assess.* **2021**, *46*, 101286.
- [46] B. Yang, H. Jiang, J. Xie, T. Zhao, Y. C. Lu, *Energy Storage Mater.* **2021**, *35*, 761.
- [47] F. Fornasiero, H. G. Park, J. K. Holt, M. Stadermann, P. Grigoropoulos, A. Noy, O. Bakajin, *Proc. Natl. Acad. Sci. U. S. A.* **2008**, *105*, 17250.
- [48] R. L. Lord, M. H. Baik, *Inorg. Chem.* **2008**, *47*, 4413.
- [49] R. E. Moran, *More Cyanide Uncertainties*, Mineral Policy Center, USA **1998**, p. 16.
- [50] L. F. Arenas, C. Ponce de León, F. C. Walsh, *J. Energy Storage* **2017**, *11*, 119.
- [51] S. Nitopi, E. Bertheussen, S. B. Scott, X. Liu, A. K. Engstfeld, S. Horch, B. Seger, I. E. L. Stephens, K. Chan, C. Hahn, J. K. Nørskov, T. F. Jaramillo, I. Chorkendorff, *Chem. Rev.* **2019**, *119*, 7610.
- [52] E. A. Heintz, *J. Inorg. Nucl. Chem.* **1961**, *21*, 262.
- [53] J. H. Bigelow, J. C. Bailar Jr., *Inorganic Syntheses*, McGraw-Hill, New York **1946**.
- [54] M. J. Frisch, G. W. Trucks, H. B. Schlegel, M. J. Frisch, G. W. Trucks, H. B. Schlegel, G. E. Scuseria, M. A. Robb, J. R. Cheeseman, G. Scalmani, V. Barone, B. Mennucci, G. A. Petersson, *Gaussian 09, Revision A. 02*, Wallingford CT, USA **2016**.
- [55] C. Lee, E. Yang, R. G. Parr, *Phys. Rev. B* **1988**, *37*, 785.